Theoretical Study on Scission Configurations of Fissioning ^{240}Pu and ^{242}Pu[†]

W. Nörenberg

Institut für Theoretische Physik der Universität Heidelberg, Heidelberg, Germany

(Received 31 August 1971)

The scission configuration is described by two interacting fragments in a single-particle model with pairing correlations and studied as function of two parameters. One parameter is the distance between the fragment centers of mass and the other parameter is the mass ratio of the two fragments. The scission-point region can be conveniently studied in this molecular model, particularly because extensive knowledge about the fragment structure is incorporated. Level schemes, equilibrium deformations of the fragments, total energies, and charge distributions are studied for the compound systems ^{240}Pu and ^{242}Pu. The scission configurations are characterized by an approximate cancellation of the attractive nuclear force and the repulsive Coulomb force between the fragment. The proton numbers of the fragments turn out to be a rather good quantum number at scission. The results support the existence of a potential barrier at the scission point (scission barrier). It is shown that the calculated energies of the scission configurations can account for the asymmetry in the fragment-mass yield with its maximum at the heavy-fragment mass $A_1 \approx 140$. The decrease of the total energy for $A_1 \approx 140$ is due to single-particle states which have a small angular momentum component along the symmetry axis and — because of their prolate density distribution — give large contributions to the binding energy between the fragments. The 50-proton shell closure has its greatest influence on the scission configuration around $A_1 = 130$, whereas the 82-neutron shell closure is most effective around $A_1 = 135$.

I. INTRODUCTION

The fission process involves large changes of the nuclear shape. Starting from a nearly spherical shape the compound nucleus strongly deforms and finally splits into two fragments with comparable masses. This process of deformation seems to be rather well understood up to the saddle point. Great progress was obtained in the last few years by the discovery of fission isomers and intermediate resonances which can be explained with the existence of a second minimum in the potential energy of the compound nucleus as function of deformation.[1] But the fission dynamics between the saddle and the scission point remains unknown. On the other hand, it is rather likely that several fission phenomena (at least for those compound nuclei which are heavier than Ra) are not determined at the saddle point but at the later stages of the fission process near the scission point.

Several models have been introduced for the discussion and calculation of fission phenomena. Among these the *adiabatic model* seems to be best suited to serve as a basis for understanding the fission process.[2] The adiabatic model is characterized by the assumption that the single-particle motion follows the collective motion adiabatically without the excitation of single-particle degrees of freedom. In order to make this assumption strictly valid, the collective motion needs to be

sufficiently slow as compared to the single-particle motion.[3] From liquid-drop-model calculations[4,5] one obtains 10^{-21} to 10^{-20} sec for the time which the compound system needs to get from the saddle to the scission point in the fission process. Critical investigations[3,6] of the adiabatic assumption cast some doubts on the general validity of the adiabatic model: Nonadiabatic transitions may be especially important near the scission point.

The following *qualitative picture of the fission process* between the saddle and the scission point is assumed: The ordered fission motion, which is described by one of the deformation parameters, is expected to be strongly damped by the coupling to other collective degrees of freedom. Additional damping may be due to the coupling to noncollective degrees of freedom. Experiments on the angular distribution of fission fragments[7] have shown that the coupling is limited to states with the same K quantum number as postulated by Bohr.[8] K measures the component of the total angular momentum along the symmetry axis of the compound system. According to the strong coupling of the ordered fission motion to other presumably collective degrees of freedom, the compound system is expected to fission through rather complicated scission configurations.

In this paper these scission configurations will be studied in some detail. The model is described

in Sec. II. In Sec. III the results of the numerical calculations are presented and discussed. Some concluding remarks are made in Sec. IV.

II. STATIONARY MOLECULAR SINGLE-PARTICLE MODEL

Scission-point configurations are successfully described by two interacting fragments. Such a configuration strongly resembles a diatomic molecule, where the atoms are replaced by the fragments. This *molecular model of fission* has been frequently used in the framework of the liquid-drop model.[9] In these calculations the nuclear interaction between the fragments is neglected. The scission-point configuration is defined by the two adjacent fragments with axial symmetric deformation. The analysis of the experimental kinetic energies and excitation energies of the fragments within such molecular models has demonstrated the influence of the fragment shell structure on the scission-point configuration. Shell effects have been explicitly studied by Ignatyuk[10] in the framework of the Nilsson model and by Dickmann and Dietrich[11] with additional Strutinsky renormalization of the total binding energy.

In this paper a single-particle model of the molecular configuration is used where the nuclear interaction between the two partly overlapping fragments is taken into account. This model had been used earlier to calculate the charge distribution[12] and the moments of inertia[13] at scission. A similar model has been studied recently by Mosel and Scharnweber.[14]
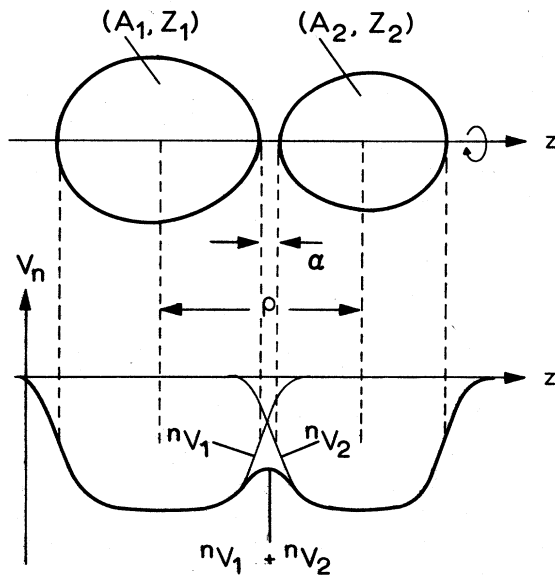

FIG. 1. The shapes of the interacting fragments and the local part of the nuclear potential V_n on the symmetry axis z.

The compound nucleus (mass number A, proton number Z, neutron number N) is described by two interacting fragments (A_1, Z_1) and (A_2, Z_2) separated by the distance ρ between the fragment centers of mass as shown in Fig. 1. This model has been formulated within the Hartree-Fock-Bogoliubov (HFB) theory[12] where one starts from an effective Hamiltonian $\mathcal{3C}$ with two-body interactions $\mathcal{v}(i, j)$ and describes the *ground state* by a BCS *wave function*

$$| \phi \rangle = \prod_{\alpha} (u_\alpha + v_\alpha a_\alpha^\dagger a_{\bar{\alpha}}^\dagger) | 0 \rangle . \qquad (1)$$

Here $| 0 \rangle$ and $a_\alpha^\dagger, a_\alpha$ denote the vacuum state and the Fermi creation and annihilation operator of the single-particle state $| \alpha \rangle$, respectively. v_α and $u_\alpha = (1 - v_\alpha^2)^{1/2}$ are real probability amplitudes for the pair of states $| \alpha \rangle, | \bar{\alpha} \rangle$ to be occupied or unoccupied. $| \bar{\alpha} \rangle$ denotes the time-reversed state with respect to $| \alpha \rangle$. The single-particle functions $| \alpha \rangle$ are expanded in terms of a finite set of the eigenfunctions $| p \rangle$ of the unperturbed spherical fragments,

$$| \alpha \rangle = \sum_p c_{\alpha p} | p \rangle . \qquad (2)$$

Variations of the total energy $\langle \phi | \mathcal{3C} | \phi \rangle$ with respect to $c_{\alpha p}$ and v_α yield a coupled set of equations which is simplified by replacing the self-consistent field by the sum $V_1 + V_2$ of the effective single-particle potentials of the fragments and by approximating the *pairing interaction* in the form

$$\langle \alpha \bar{\alpha} | \mathcal{v} | \beta \bar{\beta} \rangle - \langle \alpha \bar{\alpha} | \mathcal{v} | \bar{\beta} \beta \rangle = -\sum_{F=1}^{2} G_F w_\alpha^F w_\beta^F \qquad (3)$$

with the fragment pairing constants

$$G_F = 29 A_F^{-1} \text{ MeV} \quad \text{for neutrons}$$
$$= 32 A_F^{-1} \text{ MeV} \quad \text{for protons} . \qquad (4)$$

w_α^F is the probability that a nucleon in the state $| \alpha \rangle$ belongs to the fragment F. This probability is defined somewhat arbitrarily by

$$w_\alpha^F = \frac{1}{2} \sum_{p,q} \delta_{F(p),F} (c_{\alpha p}^* c_{\alpha q} \langle p | q \rangle + \text{conj. compl.}),$$
$$(5)$$

where $F(p)$ is 1 or 2 according to whether $| p \rangle$ is centered in the fragment 1 or 2. Expression (5) is a natural generalization of the corresponding expression

$$w_\alpha^F = \sum_p | c_{\alpha p} |^2 \delta_{F(p),F} \qquad (6)$$

for nonoverlapping fragments. The definition (5) includes one half of the overlap in w_α^1 and the other half in w_α^2, resulting in $w_\alpha^1 + w_\alpha^2 = 1$. Equation (3) takes account of the fact that the pairing interaction has to vanish if the functions $| \alpha \rangle$ and $| \beta \rangle$

are located in different nonoverlapping fragments.

With these approximations the set of *HFB equations* becomes[12]

$$\sum_q [\langle p|H|q \rangle + (-)^{F(p)} \delta_{F(p),F(q)} \mu_- - \eta_\alpha \langle p|q \rangle] c_{\alpha q} = 0, \tag{7}$$

$$v_\alpha{}^2 = 1 - \mu_\alpha{}^2 = \tfrac{1}{2} \{1 - (\eta_\alpha - \mu_t)[(\eta_\alpha - \mu_t)^2 + \tilde{\Delta}_\alpha{}^2]^{-1/2}\}, \tag{8}$$

$$\tilde{\Delta}_\alpha = w_\alpha^1 \, {}^t\Delta_1 + w_\alpha^2 \, {}^t\Delta_2, \tag{9}$$

$${}^t\Delta_F = \tfrac{1}{2} G_F \sum_\alpha^{(t)} w_\alpha^F \tilde{\Delta}_\alpha [(\eta_\alpha - \mu_t)^2 + \tilde{\Delta}_\alpha{}^2]^{-1/2}, \tag{10}$$

for neutrons $(t=n)$ and protons $(t=p)$, respectively. The Lagrange multipliers μ_- and μ_t have to be determined according to the constraints of constant fragment-mass difference $A_1 - A_2$ and constant total number of neutrons N and protons Z. η_α are the *level energies* of the single-particle states. ${}^t\Delta_F$ can be interpreted as the *gap parameter of the fragment F*. The index t in Eq. (10) indicates that the sum is taken over neutron states $(t=n)$ or proton states $(t=p)$, only. The single-particle Hamiltonian H is the sum of the kinetic energy T and the two fragment potentials V_1 and V_2. These potentials V_F are functions of the mass A_F, charge Z_F, and two deformation parameters ${}^F\delta_2$ and ${}^F\delta_3$ which describe the *axial-symmetric quadrupole and octupole deformations* of the fragments.[12] The *fragment mass A_F* and *charge Z_F* are functions of $c_{\alpha p}$ and v_α:

$$A_F = \sum_\alpha v_\alpha{}^2 w_\alpha^F, \tag{11}$$

$$Z_F = \sum_\alpha^{(p)} v_\alpha{}^2 w_\alpha^F. \tag{12}$$

The set of HFB Eqs. (7)–(10) is solved self-consistently in A_F and Z_F by iteration. More details of the model(e.g. the volume-conservation condition) are presented in Ref. 12. But several improvements over these early calculations have to be mentioned.

The *fragment potential V_F* consists of a Coulomb part and a nuclear part. The local part of the latter is taken to be of the Woods-Saxon form as indicated in Fig. 1. In Ref. 12 the matrix elements $\langle p|V_{F'}|q \rangle$ with $F(p) = F(q) \ne F'$ have been calculated by approximating the nuclear as well as the Coulomb part by two appropriate Gaussians. Whereas this approximation is good for the Coulomb potential in the region of interest, it is rather bad for the nuclear potential because of the large surface thickness of the Gaussian. The calculation of the nuclear matrix elements has been improved by approximating the deformed Woods-Saxon po-

tential [potential depth 50 MeV, diffuseness parameter 0.7 fm, half-density radius $R(\delta_\lambda, \theta)$ as defined in Eq. (A5) of Ref. 12] by a Gaussian multiplied with a sixth-order polynomial which reproduces the Woods-Saxon potential in the region of overlap within 5% of the central value.

The *total energy* is calculated according to the following expression:

$$E_t \equiv \langle \phi|\mathcal{H}|\phi \rangle \approx \sum_\alpha v_\alpha{}^2 \langle \alpha|H - \tfrac{1}{2}(V_1 + V_2)|\alpha \rangle + E_{\text{pair}}, \tag{13}$$

where the pairing energy is given by

$$E_{\text{pair}} = -\sum_{F=1}^{2} \sum_{t=p,n} \left[\frac{{}^t\Delta_F{}^2}{{}^t G_F} + {}^t G_F \sum_\alpha^{(t)} v_\alpha{}^4 (w_\alpha^F)^2 \right]. \tag{14}$$

The minimum of the total energy with respect to variations of the deformation parameters ${}^1\delta_2$, ${}^1\delta_3$, ${}^2\delta_2$, and ${}^2\delta_3$ determines the *equilibrium state of the compound system* for given values of the distance ρ between the fragment centers of mass and of the fragment masses A_1 and $A_2 = A - A_1$. It is assumed that reasonable values for the energy differences for constant A_1 can be obtained by this method. Around the scission point these energy differences are produced by the rather small perturbations of the fragments due to their mutual interaction. Only those single-particle states which are near to the Fermi energy, essentially contribute to these energy differences. The low-lying single-particle states give contributions to the Coulomb part of the energy differences, only.

Useful quantities in the discussion of scission configurations are defined by

$$\begin{Bmatrix} N_n \\ Z_n \end{Bmatrix} = \sum_\alpha^{\{{}^n_p\}} v_\alpha{}^2 (1 - |w_\alpha^1 - w_\alpha^2|), \tag{15}$$

where the sum goes over neutron and proton states, respectively. For well-separated fragments with no degeneracy of levels in different fragments these quantities vanish. N_n and Z_n measure to some extent the number of neutrons and protons belonging to both fragments simultaneously. Therefore they are called *neck neutrons* and *neck protons* although these quantities are not observables and differ considerably from the classical picture.

III. RESULTS OF THE NUMERICAL CALCULATIONS AND DISCUSSION

In the numerical calculations for ^{240}Pu and ^{242}Pu the expansion, Eq. (2), is limited to states $|p\rangle$ which have energies (including the first-order perturbation correction due to the other fragment) less than 5 MeV above the Fermi energy. In addition, the expansion is simplified by assuming

$c_{\alpha p} = \delta_{\alpha p}$ for states lying more than 5 MeV below the Fermi energy. Thus mixing is allowed only between states which lie within a region of about 10 MeV around the Fermi energy. It has been shown[13] that this limitation of the configuration space has practically no influence on the collective features of the total wave functions in the re-gion of fragment distances ($\rho \gtrsim 14$ fm) which cor-respond to the scission configurations. A *two-pa-rameter study* has been performed for various quantities of the scission configurations. The pa-rameters are the center-to-center distance ρ be-tween the two fragments and the mass A_1 of one of the fragments which fixes the mass ratio A_1/A_2,
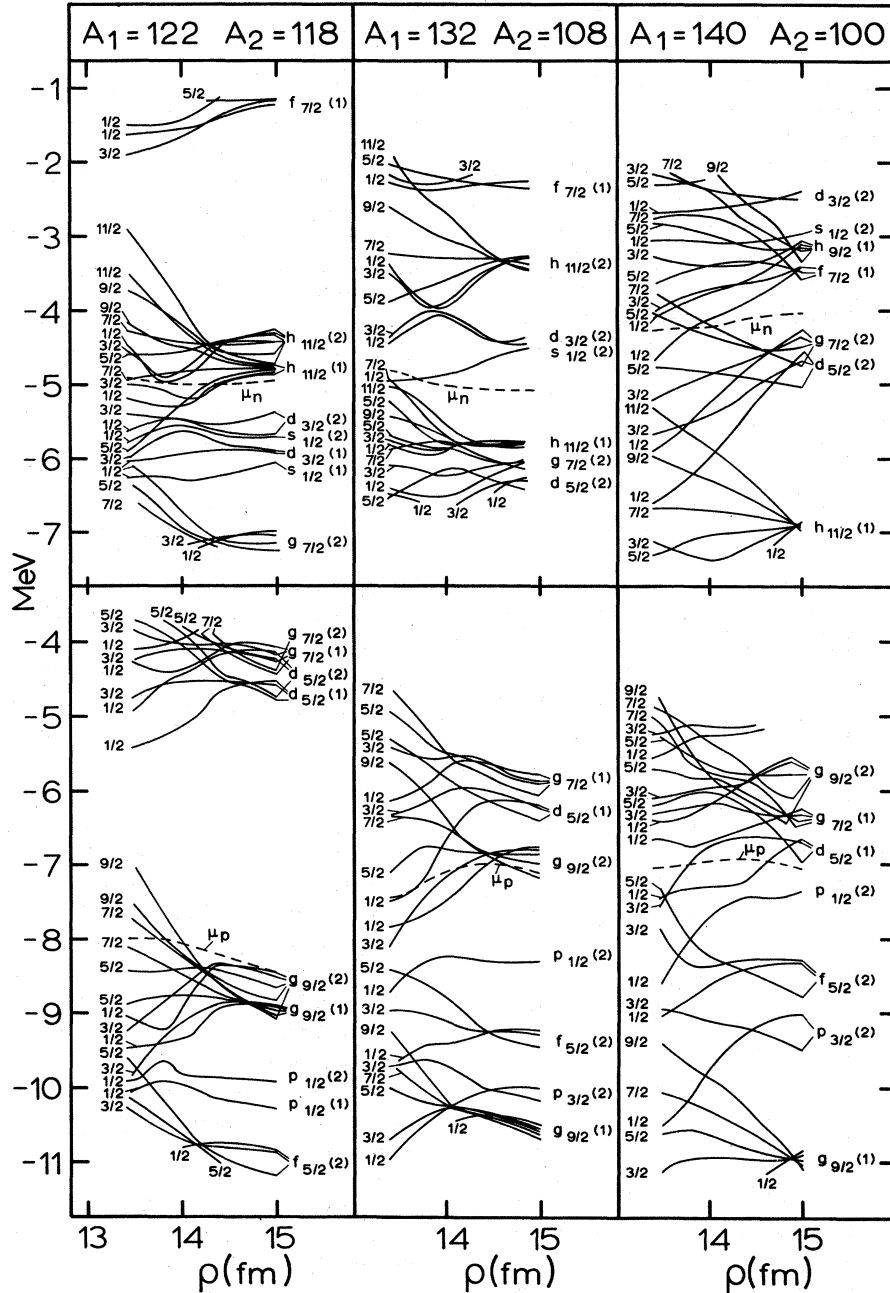

FIG. 2. ^{240}Pu: Neutron (upper half of the diagram) and proton (lower half) levels η_α as functions of ρ for the three fragment pairs $(A_1, A_2) = (122, 118)$, $(132, 108)$, and $(140, 100)$. Each level is labeled by the component m of the angular momentum along the symmetry axis. Also given are the symptotic quantum numbers of the separated fragments where the number in parentheses indicates the fragment ($F = 1$ or 2).

since $A_2 = A - A_1$. Apart from Fig. 6 all the results are reported for the compound nucleus ^{240}Pu only, because there are no qualitative and only minor quantitative differences between the results for ^{242}Pu and ^{240}Pu.

A. Quantities as Functions of ρ

Figure 2 shows the *energy levels* η_α as functions of ρ in the vicinity of the chemical potentials μ_n and μ_p (i.e., essentially in the vicinity of the Fermi energy) for three pairs of fragment masses. To make the graphs as transparent as possible, fluctuations in the curves which are usually less than 0.1 MeV have been suppressed. The diagrams clearly display the mixing and perturbation of the single-particle states caused by the interaction between the fragments. Levels with the same component m of the angular momentum along the symmetry axis do not cross. In the region 14.2 fm $< \rho$ < 14.8 fm the influence of the nuclear interaction
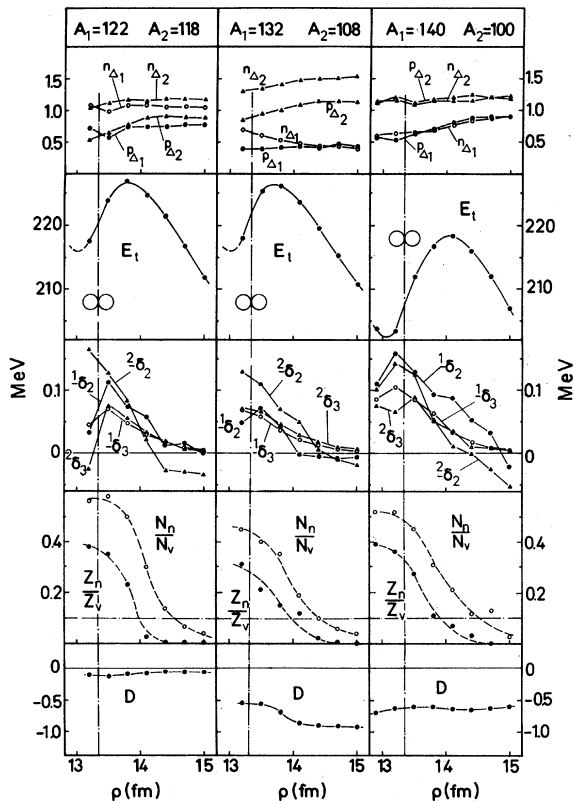

FIG. 3. ^{240}Pu: gap parameters $^n\Delta_F$ and $^p\Delta_F$ for neutrons and protons, respectively; total energy E_t; deformation parameters $^F\delta_2$ and $^F\delta_3$; relative number of neck neutrons N_n/N_v and neck protons Z_p/Z_v; and charge deviation $D(\rho, A_1)$ from the unchanged charge density (UCD) distribution as function of ρ for the three fragment pairs $(A_1, A_2) = (122, 118)$, $(132, 108)$, and $(140, 100)$.

on the level structure is approximately compensated by the Coulomb interaction. Because of this direct Coulomb interaction between the fragments *the cancellation of nuclear and Coulomb interaction* occurs at somewhat smaller values of ρ for protons than for neutrons. An interesting feature of the level schemes is connected with the *shell structure of the heavy fragment*. The shell structure gap is between the $g_{9/2}$ and the $d_{5/2}$ level group for the 50-proton shell closure and between the $h_{11/2}$ and the $f_{7/2}$ level group for the 82-neutron shell closure. At first sight, the influence of both magic shell closures is expected to be strongest for the heavy-fragment mass $A_1 = 132$. But as is seen from the diagrams, the chemical potentials μ_n and μ_p lie rather close to the $h_{11/2}$ levels for the neutrons and also rather close to the $d_{5/2}$ levels for the protons. The most pronounced shell effects are expected to occur when the chemical potential is in the middle of the gap. Therefore, the neutron and proton shell structure cannot fully develop at the same fragment mass: The proton (neutron) shell structure should have greatest influence on fission phenomena for heavy-fragment masses somewhat lighter (heavier) than 132. Because of the direct Coulomb repulsion *the proton shells are less disturbed* by the nuclear interaction between the fragments. In addition, the energy distance to the next shell is larger for the protons than for the neutrons. Therefore the 50-proton shell closure should have a more significant effect on the scission configuration than the 82-neutron shell closure. Another interesting point is connected with the *level density* near the chemical potentials. This level density turns out to be much larger for the symmetric mass splits $(A_1, A_2) = (122, 118)$ than for the asymmetric mass splits $(132, 108)$ and $(140, 100)$.

Figure 3 gives a compilation of several collective quantities as functions of ρ for three different fragment pairs:

(a) The *gap parameters* of protons $^p\Delta_1$, $^p\Delta_2$ and neutrons $^n\Delta_1$, $^n\Delta_2$ as defined in Eqs. (9) and (10) do not significantly depend on ρ. Due to the mixing between the single-particle states of different fragments, the pairing gaps $^n\Delta_1$ and $^p\Delta_1$ of the near-magic fragment with $A_1 = 132$ do not drop to zero for $\rho \leqslant 15$ fm.

(b) The *total energy* E_t minimized with respect to the deformations exhibits a *scission barrier* near $\rho = 13.8$ fm for all three pairs of fragments. At the maximum of this scission barrier the attractive nuclear force between the fragments is compensated by the repulsive Coulomb force. This cancellation occurs at distances of the fragment centers of mass where only the tails of the density distribution of the two fragments overlap. Figure

1 is a realistic picture of this configuration: If one would describe the fragments by liquid drops with equivalent deformations, the distance a between the sharp surfaces is ≈ 1.2 fm. Only at $\rho \leqslant 13.4$ fm the liquid-drop surfaces of the fragments come into contact as indicated by two touching spheres in Fig. 3. Therefore the reason for the scission barrier to occur seems to be entirely due to the diffuseness of the fragment surfaces and to the finite range of the nuclear interaction. Results on this scission barrier have been published earlier.[15] In order to use the model to some extent also for $\rho \leqslant 13.4$ fm, the saturation property of nuclear matter was approximately taken into account by imposing a constraint on the deformation parameters:

$$\rho = R_1(^1\delta\lambda, \ \theta = 0) + R_2(^2\delta\lambda, \ \theta = \pi), \qquad (16)$$

with the half-density radius $R_F(^F\delta\lambda, \theta)$ used in the definition of the Woods-Saxon potential which is discussed in Sec. II, between Eqs. (12) and (13). This constraint prevents the total nuclear potential from exceeding the saturation value. The barrier maximum may be used to *define the scission point* unambiguously. The energy curves have been normalized to the Coulomb energy of two point charges at $\rho = 15$ fm. Normalized in this way, the energy of the scission-barrier top should be equal to the experimental value of the total kinetic energy of the fragments. Thereby it is assumed that the kinetic energy at the barrier top is close to zero and that during the separation process past this point the fragments are not excited. This energy is approximately 30 MeV too high as compared to the experimental value.[16] The dipole polarization energy of the individual fragments which is not included would bring the energy of the barrier closer to the experimental kinetic energy. In addition a more realistic value for the nuclear radii of the fragments ($1.25A_F^{1/3}$ fm instead of $1.20A_F^{1/3}$ fm which has been used here[12]), and the actual excitation of the fragments along the way down from the top of the barrier would also reduce the final kinetic energy of the fragments. It is expected that the scission barrier is 10 to 20 MeV below the saddle point. No indication for the experimental dip in the kinetic energy at symmetric mass division is observed.

(c) The diagrams of the next row in Fig. 3 display a strong dependence of the *deformation parameters* $^1\delta_2$, $^1\delta_3$, $^2\delta_2$, and $^2\delta_3$ on the center-to-center distance ρ of the fragments. With increasing ρ the fragment deformations change from prolate ($-^F\delta_2 > 0$) to oblate ($-^F\delta_2 < 0$) shapes. As is seen from the middle diagram, the near magic

fragment ($A_1 = 132$) becomes almost spherical for a rather small value of ρ, namely ≈ 14.0 fm. It is interesting to note that for the near symmetric mass division ($A_1 = 122, A_2 = 118$) the lighter fragment prefers oblate shapes for $\rho > 14.2$ fm, whereas the heavier fragment remains prolate up to $\rho = 15$ fm. This indicates a strong coupling of the mass-asymmetry vibration with the distortion-asymmetry vibration (notation according to Nix[4]) for near symmetric mass splits. For $\rho \leqslant 13.4$ fm the constraint on the deformation parameters discussed above becomes obvious.

(d) The *number of neck nucleons* as defined by Eq. (15) also depends rather strongly on ρ. In Fig. 3 the ratio of the neck nucleons (Z_n, N_n) to valence nucleons (Z_v, N_v) is shown, the valence nucleons being defined by the total number of protons and neutrons, respectively, occupying the fragment functions $|p\rangle$ within 10 MeV around the Fermi energy. The number of the valence nucleons are $Z_v = 38, 26, 34$ and $N_v = 46, 56, 42$ for the fragment pairs $(A_1, A_2) = (122, 118)$, $(132, 108)$, and $(140, 100)$, respectively. The most striking feature of these graphs is the small number of neck protons as compared to the number of neck neutrons. Such an effect is expected from the direct Coulomb repulsion which shifts the protons somewhat to the outer edges of the fragments (dipole polarization of the fragments). The ratio Z_n/Z_v of the protons reaches a value of 0.1 near $\rho = 14.0$ fm, whereas the ratio N_n/N_v reaches this value only near $\rho = 14.5$ fm. From this it may be concluded that the *number Z_F of protons in the fragments is at the scission point a rather good quantum number* and at least much better than the number N_F of neutrons or the total number $A_F = N_F + Z_F$ of nucleons.

(e) To characterize the *fragment charge Z_F* as defined by Eq. (12), the *deviation*

$$D(\rho, A_1) \equiv Z_1(\rho, A_1) - A_1 Z/A = -D(\rho, A_2), \qquad (17)$$

from the unchanged charge density (UCD) distribution is plotted as a function of ρ. For the fragment pairs $(A_1, A_2) = (122, 118)$ and $(140, 100)$ the charge distribution is constant as function of ρ. For $(A_1, A_2) = (132, 108)$ a *shell effect* on the charge distribution is seen to develop around $\rho = 13.8$ fm, which is the scission point as defined by the top of the scission barrier. As indicated by the relatively small number of neck protons and by the level diagrams of Fig. 2, the proton shell structure is expected to be more effective than the neutron shell structure. Therefore a larger effect on the charge distribution is expected from the 50-proton shell than from the 82-neutron shell, which is demonstrated below in Figs. 5 and 6.

B. Quantities as Functions of A_1

There are several experiments where fission phenomena are studied as functions of the fragment masses, e.g., the heavy-fragment mass. It is therefore interesting to examine some features of the scission configuration also as functions of the heavy-fragment mass A_1. As is seen from the

energy curves in Fig. 3, the barrier top, which is suited to serve as a definition of the scission point, occurs at $\rho \approx 13.8$ fm. Therefore, ρ is set equal to 13.8 fm in the following study of some quantities as functions of A_1.

In Fig. 4 the *levels*, which have been shown in Fig. 2 as functions of ρ, are drawn as functions of A_1 for $\rho = 13.8$ fm. As in the corresponding dia-
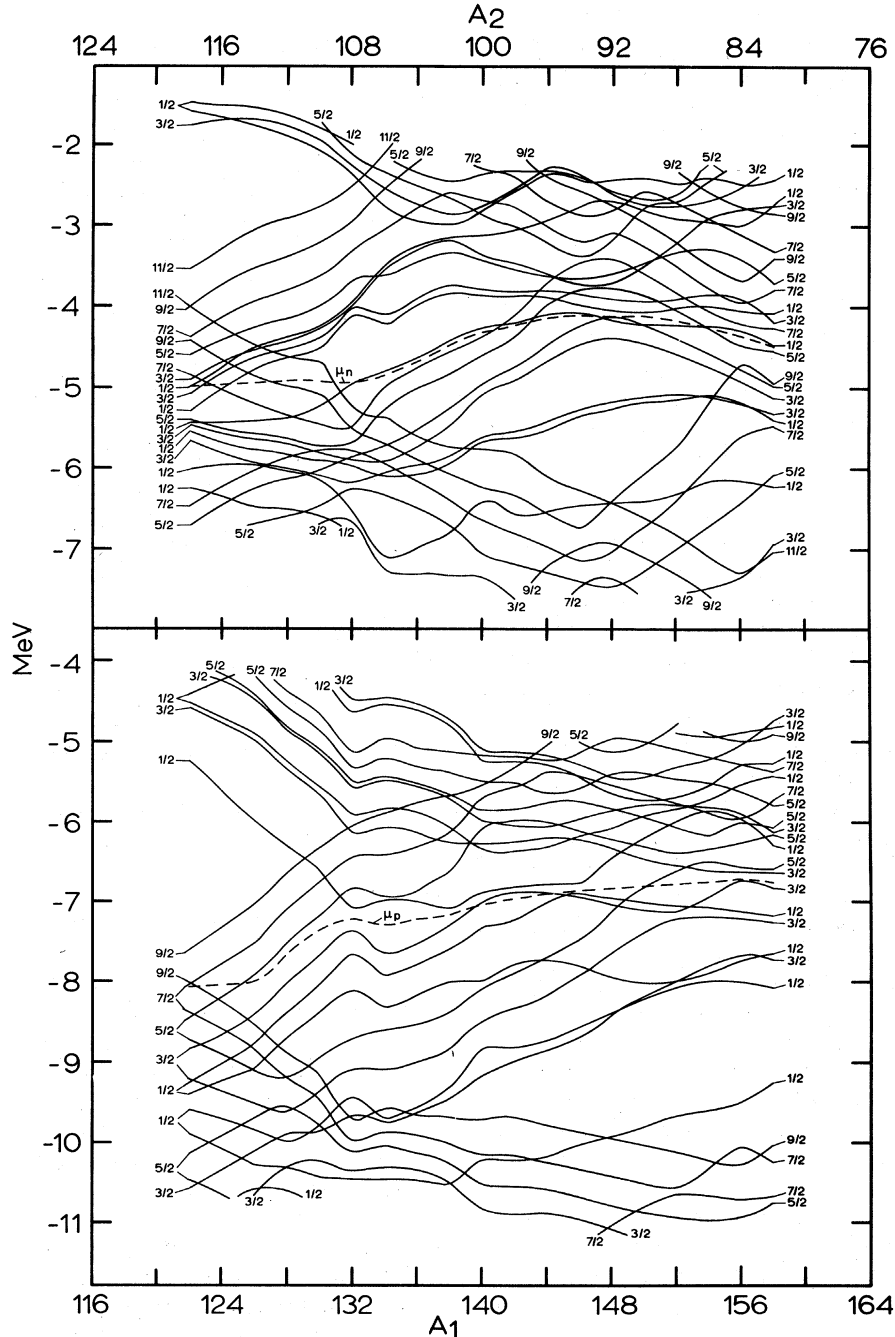

FIG. 4. ^{240}Pu: neutron (upper half of the diagram) and proton (lower half) levels η_α as functions of A_1 for $\rho = 13.8$ fm. Each level is labeled by the component m of the angular momentum along the symmetry axis.

grams of Fig. 2, fluctuations of the order of 0.1 MeV in the curves have been suppressed. These level diagrams exhibit some interesting features: In the symmetric mass region $A_2 \lesssim A_1 \lesssim 128$ states with a large angular momentum component m along the symmetry axis dominate near the chemical potentials μ_n and μ_p. Because of their oblate spatial density distribution, these states with large m have almost no overlap with the density distribution of the other fragment and therefore give no essential contribution to the binding energy of the compound system. On the other hand, several states with small m values are populated for $A_1 \approx 140$ which give a large contribution to the binding energy according to their prolate density distribution. That there is *more binding energy with the fragment pair (140, 100)* is evident in the total energy curve of Fig. 3. In particular the can-

cellation of nuclear attraction and Coulomb repulsion is at 14.0 fm, whereas for the other fragment pairs this point occurs at 13.8 fm.

In Fig. 5 are presented the deformation parameters, the gap parameters, and the charge distribution as functions of A_1 for $\rho = 13.8$ fm:

(a) The *quadrupole deformation* parameter $^F\delta_2$ displays strong variations between 0.04 and 0.14. A *shell effect* is realized around mass $A_1 = 132$ in the quadrupole deformation $^1\delta_2$. The *octupole deformation* parameter $^F\delta_3$ is rather constant (≈ 0.05) aside from small fluctuations. The fragments are always pear-shaped pointing with their sharper tips to each other as indicated in Fig. 1. It should be stressed that these deformation parameters belong to the top of the scission barrier (see Fig. 3). Because of the partial cancellation of nuclear attraction and Coulomb repulsion between the fragments, the *deformations are rather small* at this point. This supports the usefulness of the model for studying the scission configuration. The deformations of the scission point given in Fig. 5 cannot be compared with those calculated by Dickmann and Dietrich[11] who have chosen the touching spheroid configuration as the scission point. Because of our limitation of the configuration space, the deformations are expected to be too small by a factor of 1.5 or 2 at this touching point (see Fig. 3).

(b) The *gap parameters* clearly display *shell effects* for the heavy fragments near $A_1 = 132$. As has already been expected from the level diagrams of Fig. 2, the proton shell effect is largest for heavy-fragment masses somewhat lighter than 132, namely 130; whereas for the neutrons it is for somewhat heavier fragments, namely 134 and 136.

(c) The calculated *charge distribution* is given by the points connected by a line. For $A_1 = 122$, 132, and 140 the variance of the calculated values,
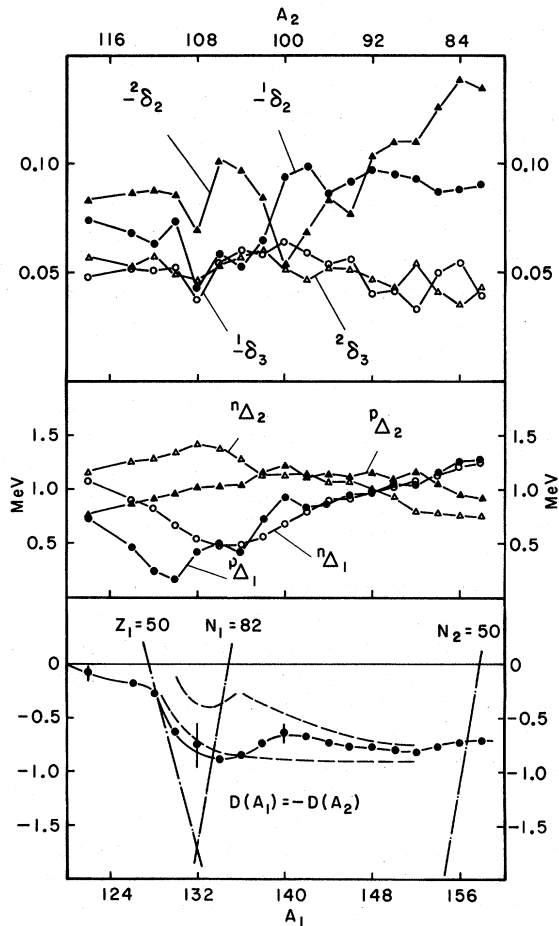

FIG. 5. ^{240}Pu: deformation parameters $^F\delta_2$ and $^F\delta_3$, gap parameters $^n\Delta_F$ and $^p\Delta_F$ for neutrons and protons, respectively, and charge deviation $D(A_1)$ from the UCD distribution as functions of A_1. The range of experimental data (Ref. 17) of the charge distribution has been indicated by the broken lines.
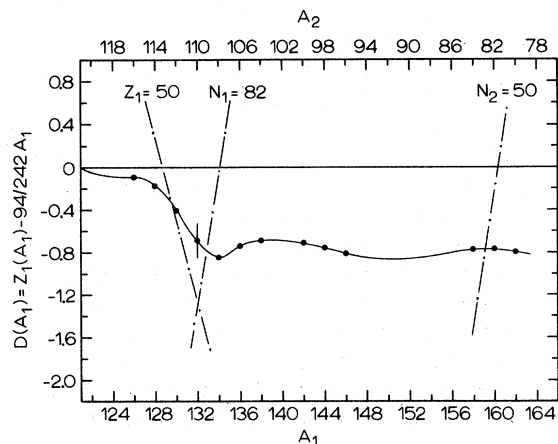

FIG. 6. Charge-distribution curve for ^{242}Pu.

taken from Fig. 3, is indicated. Again the *50-proton shell is more effective than the 82-neutron shell*. Apart from the discrepancy of 0.2 to 0.3 charge units around $A_1 = 132$ good agreement with the experimental charge distribution[17] is obtained.

Figure 6 presents the *charge-distribution curve for ^{242}Pu*. Apart from some quantitative differences to the corresponding diagram of Fig. 5, the charge distribution is the same as for ^{240}Pu.

IV. CONCLUSIONS

A rather simple model of two interacting fragments, which is described in a single-particle theory with residual pairing interaction, has been used to study some features of the scission configuration. Level schemes, equilibrium deformations of the fragments, total energies, and the charge distribution have been studied as functions of two parameters, namely as functions of the fragment masses A_1, A_2 and of the center-to-center distance ρ of the fragments. This molecular model is *convenient for studying the scission-point region*, particularly because extensive knowledge about the fragment structure is incorporated. For smaller values of ρ the configuration space in the expansion (2) has to be enlarged considerably and special care has to be taken of saturation problems. Higher multipole deformations of the individual fragments should be used. In studying these regions of smaller ρ values, two-center potentials[18] should be used and the total energy should be renormalized according to Strutinsky's method[19] to account for the saturation of nuclear matter. On the other hand one has to be careful when using the renormalization with liquid-drop energies for fragment distances ρ in the region of the scission barrier. Large errors are introduced there, since the nuclear interaction energy between the fragments is "renormalized" to zero according to the fact that the corresponding liquid drops are well separated (see Figs. 1 and 3).

As a main result of the calculations the scission configurations are characterized by an *approximate cancellation of the attractive nuclear force and the repulsive Coulomb force between the two fragments*. Results of this interplay of the nuclear and Coulomb interaction are the *scission barrier* and the *rather small deformations* near the barrier top. Because of the direct Coulomb repulsion the protons are shifted somewhat to the outer edges of the fragments. Thus the *number Z_F of protons* in the fragments seems to be a *much better quantum number* than the neutron number N_F or the mass number $A_F = N_F + Z_F$. From this it seems desirable to study the fission phenomena as functions of Z_F instead of A_F. In addition Z_F

is not altered by the subsequent neutron and γ emission and changes only by the very slow β decay of the fragment. Experiments of this kind have been started.[20] In addition the 50-proton shell has a much greater influence on some features of the scission configuration than the 82-neutron shell.

The great disadvantage, which is common to all stationary models of fission, is the fact that the *fission dynamics between the saddle and the scission configuration is not considered explicitly*. As mentioned in the Introduction, the compound system probably fissions through rather complicated scission configurations. It is expected that these complicated scission configurations can be built up approximately from the ground-state scission configuration by particle-hole or quasiparticle excitations. It is reasonable that some collective features of the ground-state scission configuration are the same, at least on the average, for these complicated scission configurations. But there remains another objection with these calculations: Since almost nothing is known about the dynamical path, it is possible that the compound system cannot reach all equilibrium states of the scission configurations. Therefore also *other scission configurations* which are rather different in deformation and structure may be effective. On the other hand, it is a very difficult problem to give a realistic solution to the fission dynamics. Even if one assumes the validity of the adiabatic model, a solution seems to be almost impossible, since one has to use a rather large number of essential degrees of freedom (10 to 15 at least) which are expected to couple strongly to the ordered fission motion. There are serious doubts, if dynamical calculations with 2 or 3 degrees of freedom[4,5] can give a reasonable answer to this problem.

An interesting result of the calculations is the *existence of a scission barrier*. Such a barrier has been proposed in connection with several discussions on fission phenomena.[21-23] This barrier occurs at distances where only the *tails of the density distribution* of the two fragments overlap. Consequences of such a barrier on fission dynamics and on the existence of fission isomers in the scission valley inside the barrier have been discussed elsewhere.[15] The relative heights of the barriers can be renormalized by using a mass formula. From the mass table given by Garvey et al.[24] the values 3, −1, and 0 MeV for the barrier heights of the fragment pairs $(A_1, A_2) = (122, 118)$, $(132, 108)$, and $(140, 100)$ are obtained. For the valleys the corresponding values are 8.5, 4.5, and 0 MeV. In the *thermodynamic molecular model*[22,25] a statistical equilibrium of collective states

is expected in the scission valley. According to this model the probability of finding a specific fragment pair is determined by the Boltzmann factor,

$$P_v(A_F) \sim \exp[-E_v(A_F)/(kT_c)], \qquad (18)$$

where $E_v(A_F)$ is the energy of the valley as function of A_F, T_c is the collective temperature of the statistical equilibrium, and k is the Boltzmann constant. In order that a special fragment pair can fission, the energy in the fission degree has to be at least equal to the barrier height $E_b(A_F)$. The probability of finding this energy in the fission degree is

$$P_b(A_F) \sim \exp[-E_b(A_F)/(kT_c)], \qquad (19)$$

and therefore the *fission probability*

$$P_f \sim P_v P_b \sim \exp\{-[E_v(A_F)+E_b(A_F)]/kT_c\}. \qquad (20)$$

For the reasonable value 2.3 MeV for kT_c,[22,25] the relative fission probabilities are

$$P_f(140):P_f(132):P_f(122) = 1:0.2:(7\times10^{-3}),$$

$$\qquad (21)$$

which is in rather good agreement with the experimental values[16] $1:0.6:(7\times10^{-3})$. No quantitative agreement can be expected, since the relative energies are expected to be at least uncertain by 2 MeV. But these numbers clearly demonstrate that the *energies of the scission configuration can account for the mass distribution* and that no tunneling process is necessary for explaining the phenomenon of asymmetric fission. Pashkevich[26] has calculated the potential surface with the help of Strutinsky's method. At scission he gets a valley depth of about 5 MeV for the most probable mass division which compares rather well with the corresponding value of 8.5 MeV obtained here.

No scission barrier is obtained by Pashkevich because of the reasons discussed above at the beginning of this section.

There remains the *puzzling dip in the kinetic energy* of the fragments[16] around the symmetric mass split. In the total energy, given in Fig. 3, no indication of such a deficiency for (A_1, A_2) = (122, 118) is seen. If one takes the presented model study as complete, one has to introduce an excitation mechanism of the fragments after the scission barrier top is passed. Such a mechanism may be connected with the high density of nearly degenerated levels from different nuclei around the Fermi energy. On the other hand, it may be possible that by our limitation of the configuration space a *more deformed scission configuration* has been missed. This more deformed state can tentatively be *connected with the binding states of small m quantum numbers* which probably are responsible for the energy minimum of the scission valley around $A_F = 140$.

Finally a remark should be made in connection with the *charge distribution* given in Fig. 5. The experimental values for $A_1 \approx 136$ indicate a more pronounced effect from the 82-neutron shell than is displayed by the charge distribution at $\rho = 13.8$ fm. This effect suggests a redistribution of neutrons beyond the scission-barrier top and may be connected with a small *Josephson junction*[26] between the fragments.

ACKNOWLEDGMENTS

†Work supported in part by the Bundesministerium für Bildung und Wissenschaft.

[1]V. M. Strutinsky and H. C. Pauli, in *Proceedings of the Second International Atomic Energy Symposium on Physics and Chemistry of Fission, Vienna, Austria, 1969* (International Atomic Energy Agency, Vienna, Austria, 1969), p. 155; J. E. Lynn *ibid.*, p. 249; Atomic Energy Research Establishment Report No. AERE-R 5891, Harwell, 1986 (unpublished).

[2]D. L. Hill and J. A. Wheeler, Phys. Rev. **89**, 1102 (1953).

[3]L. Wilets, *Theories of Nuclear Fission* (Clarendon Press, Oxford, 1964).

[4]J. R. Nix, Nucl. Phys. **A130**, 241 (1969).

[5]R. W. Hasse, Nucl. Phys. **A128**, 609 (1969).

[6]J. J. Griffin, in *Proceedings of the Second International Atomic Energy Symposium on Physics and Chemistry of Fission, Vienna, Austria, 1969* (see Ref. 1), p. 3.

[7]A. I. Obukhov and N. A. Perfilov, Usp. Fiz. Nauk **92**, 621 (1967) [transl.: Soviet Phys. – Usp. **10**, 559 (1968)]; B. D. Wilkins, J. P. Unik, and J. R. Huizenga, Phys. Letters **12**, 243 (1964); E. Albertson and B. Forkman, Nucl. Phys. **70**, 209 (1965); I. E. Bocharova, V. G. Zolotukhin, S. P. Kapitza, G. N. Smirenkin, A. S. Soldatov, and Yu. M. Tsipeniuk, Zh. Eksperim. i Teor. Fiz. **49**, 476 (1965) [transl.: Soviet Phys. – JETP **22**, 335 (1966)]; H. C. Britt, W. R. Gibbs, J. J. Griffin, and R. H. Stokes, Phys. Rev. **139**, B354 (1965).

[8]A. Bohr, in *Proceedings of the United Nations International Conference on the Peaceful Uses of Atomic Energy, Geneva, 1955* (United Nations, New York, 1956), Vol. 2, p. 151.

[9]R. Vandenbosch, Nucl. Phys. 46, 129 (1963); J. M. Ferguson and P. A. Read, Phys. Rev. 150, 1018 (1966); H. W. Schmitt, Arkiv Fysik 36, 633 (1967); J. Terrell, Phys. Rev. 127, 880 (1962); in *Proceedings of the International Atomic Energy Symposium on Physics and Chemistry of Fission, Salzburg, Austria, 1965* (International Atomic Energy Agency, Vienna, Austria, 1965), Vol. II, p. 3; P. Armbruster, Nucl. Phys. A140, 385 (1970).

[10]A. V. Ignatyuk, Yadern. Fiz. 7, 1043 (1968) [transl.: Soviet J. Nucl. Phys. 7, 626 (1968)].

[11]F. Dickmann and K. Dietrich, Nucl. Phys. A129, 241 (1969).

[12]W. Nörenberg, Ph.D. thesis, Technischen Hochschule München, 1966 (unpublished); Z. Physik 197, 246 (1966); Phys. Letters 19, 589 (1965).

[13]N. Rösch, Z. Physik 215, 368 (1968).

[14]U. Mosel and D. Scharnweber, Phys. Rev. Letters 25, 678 (1970).

[15]W. Nörenberg, Phys. Letters 31B, 621 (1970).

[16]J. N. Neiler, F. J. Walter, and H. W. Schmitt, Phys. Rev. 149, 894 (1966).

[17]S. M. Quaim and H. O. Denschlag, J. Inorg. Nucl. Chem. 32, 1763 (1970), and references cited there.

[18]M. Brack, J. Damgaard, H. C. Pauli, A. Strenholm-Jensen, V. M. Strutinsky, and C. Y. Wong, to be published; J. Damgaard, H. C. Pauli, V. V. Pashkevich, and V. M. Strutinsky, Nucl. Phys. A135, 432 (1969); B. L. Anderson, F. Dickmann, and K. Dietrich, *ibid.*

A159, 337 (1970); D. Scharnweber, W. Greiner, and U. Mosel, *ibid.* A164, 257 (1971).

[19]V. M. Strutinsky, Nucl. Phys. A95, 420 (1967); A122, 1 (1968).

[20]H. Nifenecker, M. Ribrag, J. Frehaut, and J. Gauriau, Nucl. Phys. A131, 261 (1969); H. Nifenecker, J. Frehaut, and M. Soleilhac, in *Proceedings of the Second International Atomic Energy Symposium on Physics and Chemistry of Fission, Vienna, Austria, 1969* (see Ref. 1), p. 491; L. E. Glendening, H. C. Griffin, W. Reisdorf, and J. P. Unik, *ibid.*, p. 781.

[21]H. W. Schmitt, in Proceedings of the Conference on Neutron Physics, Jülich, 1967 (unpublished), p. 7; J. O. Rasmussen, W. Nörenberg, and H. J. Mang, Nucl. Phys. A136, 465 (1969); E. Konecny, W. Nörenberg, and H. W. Schmitt, *ibid.* A139, 513 (1969).

[22]W. Nörenberg, in *Proceedings of the Second International Atomic Energy Symposium on Physics and Chemistry of Fission, Vienna, Austria, 1969* (see Ref. 1), p. 51.

[23]U. Mosel and W. Greiner, Z. Physik 222, 261 (1969).

[24]G. T. Garvey, W. J. Gerace, R. L. Jaffe, I. Talmi, and I. Kelson, Rev. Mod. Phys. 41, 1 (1969).

[25]W. Nörenberg, Habilitationsschrift, Universität Heidelberg, 1970 (unpublished).

[26]K. Dietrich, Phys. Letters 32B, 428 (1970); Ann. Phys. (N.Y.) 66, 480 (1971).

Neutron-Resonance Spin Determinations in Nd^{143} and Nd^{145} from Capture Gamma-Ray Measurements

A. Stolovy, A. I. Namenson, J. C. Ritter, T. F. Godlove, and G. L. Smith

Nuclear Sciences Division, Naval Research Laboratory, Washington, D. C. 20390

(Received 31 January 1972)

Spin assignments have been made for 47 neutron resonances in the target nuclei Nd^{143} and Nd^{145} by two independent methods: measurement of coincidences between cascade capture γ rays, and measurement of the ratio of low-energy γ-ray intensities. A new method for analyzing data of this type is introduced which enables us to assign a probability of correctness to each spin measurement. The use of an energy window rather than an integral bias level for the coincidence experiment improves the separation of the two spin groups. The s-wave strength function does not appear to be spin-dependent. The distribution of the spin values is consistent with a $2J+1$ level-density dependence.

I. INTRODUCTION

In recent years, several techniques have been developed for the determination of the spin states of s-wave neutron resonances from studies of the capture γ rays associated with the resonances. Most of these methods depend upon the assumption that the compound-nucleus state decays in a statistical manner via dipole transitions. Experiments of this type are much simpler to perform

than experiments using polarized targets and/or polarized neutrons, or methods based upon neutron scattering measurements. Spin assignments for many resonances in the same isotope are needed to determine the possible spin dependence of the s-wave strength function, the level density, the radiative capture width, and the influence of doorway and intermediate states.

The experiments based on the use of capture γ rays can be classified as follows: (1) Observation